



Influences of various parameters on shear stiffness of bolted joints subjected to shear load

Ayaka Murai¹ · Tadatoshi Watanabe² · Masahiro Fukuda¹ · Shinji Hashimura³ 

Received: 16 February 2023 / Accepted: 9 June 2023 / Published online: 6 July 2023
© The Author(s) 2023

Abstract

Parameters which affect shear stiffness characteristics of bolted joints subjected to shear load should be elucidated in order to design mechanical structures for functionality focusing not only on their strength and self-loosening but also on their shear stiffness. In this study, we have both experimentally and analytically investigated the behaviors of a bolted joint subjected to shear load and primary parameters which determine the shear stiffness characteristics of bolted joints. The experiments have been conducted applying the shear load four times repeatedly on clamped plates of a bolt/nut assembly with washers. We measured the shear stiffness of bolted joints and the shear load at which the slippage started to occur between the clamped plates. Four types of washers were used in the experiments with different contact areas on the clamped plates in order to reveal the effect of contact area of washers. We also conducted FE analysis under the same conditions. As the results, it was seen that the shear stiffness slightly increased with an increase in the clamp force of bolted joint. The shear stiffness was not influenced by the number of loading cycles. It was also seen that the amount of rotational deformation in the bolted joint depended on the slippage between the clamped plates. Although the rotation deformation was very small until the slippage occurrence, the rotational deformation remarkably increased after the slippage occurred. In general, it is well-known that the joining portion of lap jointed plates by spot welding, for example, slightly and rotationally deformed, but it has never been elucidated that the inclination angle due to the rotational deformation depends on the slippage between the clamped plates in the bolted joint. It was also seen that the shear stiffness until the slippage occurrence increased with an increase in the contacting surface area between the clamped plates. Although we investigated the effect of surface roughness of the clamped plates only in the experiments, we cannot clearly reveal its effect on the shear stiffness. But it is seen from the FE analysis result that the friction coefficient between clamped plates had a slight influence on the shear stiffness. The result shows that the shear stiffness of bolted joint mainly depends not only on the slip resistance between the clamped plates but also on increase of the contact surface between the washers and clamped plates. The results can be applied in order to control the shear stiffness of lap-jointed plates by spot welding and so on.

Keywords Bolt/nut assembly · Shear load · Shear stiffness · Clamp force · Washer · Friction coefficient · Surface roughness

1 Introduction

Multi-material structures have been required on various vehicles in order to improve fuel efficiencies by reducing weight [1, 2]. To execute multi-material structures effectively, we have to select not only the optimum material for each structure but also the optimum joining techniques for each joint. The main techniques to join dissimilar materials are bonding, various kinds of welding, friction stir joining, and mechanical joining [3–6]. Of these, the mechanical joining methods can join more kinds of materials than welding can, as it can also be applied to resin. Unlike other mechanical joining methods, the bolt tightening method can

✉ Shinji Hashimura
hasimura@shibaura-it.ac.jp

¹ Department of Mechanical Engineering, Shibaura Institute of Technology Graduate School, 3-7-5, Toyosu, Koto-ku, Tokyo 135-8548, Japan

² Technical Research Center, Mazda Motor Corporation, 3-1 Shinchi, Fuchu-cho, Aki-gun, Hiroshima 730-8670, Japan

³ Department of Engineering Science and Mechanics, Faculty of Engineering, Shibaura Institute of Technology Graduate School, 3-7-5, Toyosu, Koto-ku, Tokyo 135-8548, Japan

give preload as clamp force on clamped parts. As a result, the joining strength of bolted joints is higher than other mechanical joining methods [7, 8]. However, bolted joints need careful attention to clamp force reduction caused by loosening as well as static strength and fatigue strength. There have been many studies done on bolted joints, most of which have revealed the mechanical behavior of bolted joints when an axial load is applied to the joints. On the other hand, when a transverse load against bolt axis, that is shear load, is applied to the joints, slippage occurs on the thread surface and bearing surface and between bolted joints, which causes self-loosening as well as bolt or nut rotation and fatigue destruction. There remain some important issues to be solved [9, 10]. Yamamoto elucidated the relation between self-loosening and slippage on the bearing surface of the bolted joints subjected to axial transverse vibration [11]. Kase et al. showed the mechanism that causes self-loosening and limits sliding displacement of the bolted joints when they receive transverse vibration [12]. Izumi et al. supported the self-loosening mechanism revealed by Kase et al. by means of simulating the spiral shape of the screw thread in three dimensions to conduct FEM analysis [13]. Pai and Hess experimentally and analytically investigated self-loosening of bolted joints subjected to dynamic shear loads [14, 15]. Zhang et al. revealed an influence of abrasion on self-loosening behavior, and Hashimura et al. elucidated the influence of lubricant on self-loosening behavior [16, 17]. Dravid et al. revealed the influence of washers on self-loosening of bolted joints [18]. With experiments and FEM analysis, Pirdayr et al. showed the influence of vibration on self-loosening of screws [19]. Zhao et al. conducted research on the effect of the initial clamp force and contact states on the load change relation [20]. Fukuoka et al. reproduced the spiral shape of screw threads to conduct FEM analysis and found the characteristics of self-loosening, fatigue strength, and load change [21–23]. Hashimura and Socie and Hashimura and Kurakake clarified the different conditions of occurrence for self-loosening and fatigue destruction when bolted joints are subjected to transverse vibration and showed a method of evaluating fatigue destruction mechanism as well as fatigue strength in the case of transverse vibration [24, 25]. Thus, a lot of self-loosening studies have been conducted on bolted joints subjected to transverse load.

On the other hand, since there are many cases where tensile shear load acts on components with multiple thin plates joined together such as transportation equipment, it is essential not only to elucidate self-loosening behaviors but also to identify and control the shear stiffness of bolted joints to functionally and efficiently design machines. Spot welding and friction stir spot welding have been frequently used in the automotive manufacturing so far [26–30]. In the spot welding, nugget diameters on spot welds for thin plates

around 2 mm thick are about 7 mm, and the shear stiffness of joint portion can be easily controlled with the number of spots and their nugget size. On the contrary, since outer diameter of the bearing surface of flange nut is about 17 mm in bolted joints, it is not spatially easy to increase the number of bolted joints for improvement of the shear stiffness. Therefore, if effective parameters for the shear stiffness of bolted joints are revealed and controlled using flange of bolt and nut or washers effectively, functionally and efficiently designed machines and structures are possible. Furthermore, when parts that cannot be spot welded are joined with bolted joints, the degree of design freedom is increased. However, since slippage can occur on the joined part and thread surfaces, parameters influencing the shear stiffness of bolted joints must be investigated in detail.

In this study, we experimentally and analytically investigated the effects of various parameters on the shear stiffness of bolted joints consisting of two thin plates, a bolt, nut, and washers when subjected to tensile shear load. We elucidated the deformation mechanism of bolted joints subjected to shear load first. And then, we revealed the influences of clamp force, the size of the contact areas, surface roughness, and friction coefficient on the shear stiffness using washers with different contact areas to the clamped plates. Simultaneously, we investigated the influence on limit tensile shear load up to which no slippage occurs on the joined surface or thread surface. We also discussed what the most important parameter is for the shear stiffness of bolted joints.

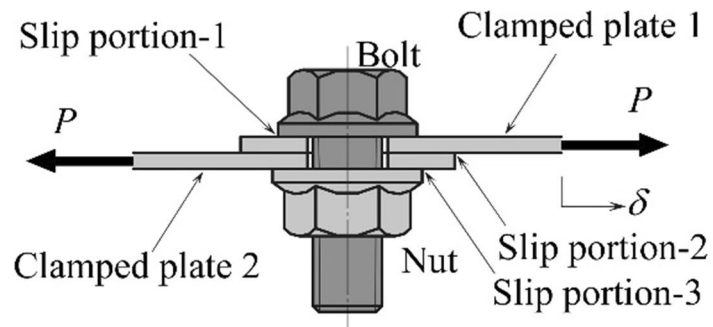
2 Shear stiffness of bolted joint

Figure 1a shows a bolted joint subjected to shear tensile force, and Fig. 1b shows a schematic illustration of the relation between relative displacement δ of clamped plates and tensile force P , based on a preliminary experiment, in which the bolted joint is subjected to tensile force P in the shear direction. When the bolted joint is pulled with P , the clamped plates are elongated at first as shown in stage I in Fig. 1b if the clamp force of the bolted joint is great enough because the tensile force P is supported by friction force generated due to the clamp force. Let the elongations of clamped plates be λ_{p-1} and λ_{p-2} , and the displacement $\delta_{\text{stage I}}$ in stage I is expressed as follows.

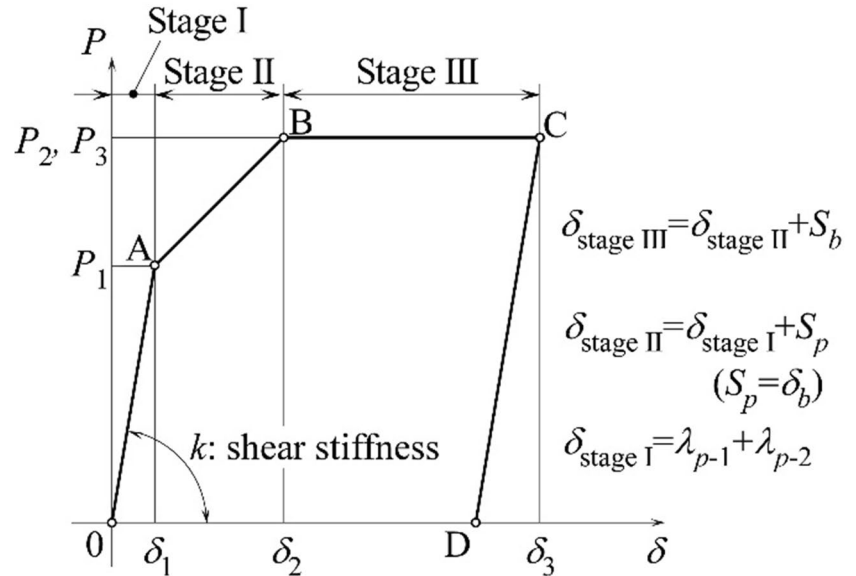
$$\delta_{\text{stage I}} = \lambda_{p-1} + \lambda_{p-2} \quad (1)$$

After that, when the tensile force P exceeds the friction force, slippage occurs at mating surfaces between the clamped parts at point A in Fig. 1b. The bolt inclines and deforms into an S-shape at that time to compensate for the relative displacement due to the slippage. That region from

Fig. 1 Bolted joint subjected to shear force and a relationship at that time between shear force and displacement



(a) Bolt/nut assembly subjected to shear force P



(b) Relationship between relative displacement δ and shear force P

point A to point B is defined as stage II. Let the slippage displacement between mating clamped plates be S_p , and the displacement $\delta_{\text{stage II}}$ in stage II is expressed by

$$\delta_{\text{stage II}} = \delta_{\text{stage I}} + S_p = \lambda_{p-1} + \lambda_{p-2} + S_p \tag{2}$$

In stage II, let the displacement due to the bolt inclination and the bolt deformation be δ_b , and δ_b equals to S_p .

Then, if the bolt deformation and inclination reach their limits at point B, the slippage occurs at the bolt-bearing surface and the nut-bearing surface. The region from point B to point C is defined as stage III in Fig. 1b. Let the slippage at the mating-bearing surface under the bolt head and the nut be S_b , and the displacement $\delta_{\text{stage III}}$ in stage III is expressed by

$$\delta_{\text{stage III}} = \delta_{\text{stage II}} + S_b = \lambda_{p-1} + \lambda_{p-2} + S_p + S_b \tag{3}$$

In Fig. 1b, the gradient from 0 to point A is defined as the shear stiffness k_1 of the bolted joint. The tensile force at

point A is defined as the limit value of elastic region force P_1 . In this study, the shear stiffness k_1 of the bolted joint and the limit value of elastic region force P_1 were measured under several conditions, and we discussed shear stiffness characteristics.

3 Experiment and finite element analysis

3.1 Bolted joints and washer types

Figure 2 shows four types of bolted joint using different washers. We prepared these washers in order to change the contact areas A_w between the washers and the clamped plates. The washers in the bolted joint in Fig. 2a were two cylindrical plain washers. We call this bolted joint as bolted joint I in this study. The washers in Fig. 2b have 60° taper shown in Fig. 2(b). We call this bolted joint as bolted joint II. The washers in Fig. 2c have a 60° taper opposite to bolted

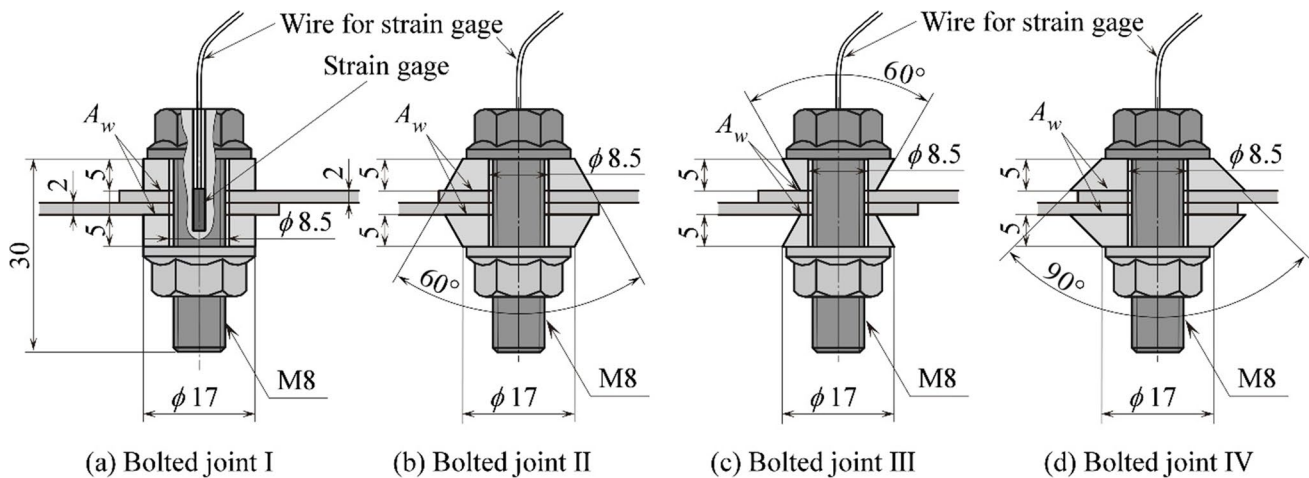


Fig. 2 Bolted joints with different washer types

joint II. We call this bolted joint as bolted joint III. The washers in Fig. 2d have 90° taper as shown in Fig. 2d. We call this bolted joint as bolted joint IV.

The nominal size and the nominal length l of the test bolt were M8 and $l = 30$ mm. The test bolt and the nut were made of medium carbon steel JIS S45C. The property class of the test bolt was 6.8. The test bolt was attached to a strain gage in the center of the bolt to measure clamp force as shown in Fig. 2a. The test nut for all bolted joints was a commercial hexagon head bolt M8 with flange. Each dimension is shown in Fig. 2. The grip length l_g that is the length between the bearing surface under the bolt head and the bearing surface under the nut was $l_g = 14$ mm for all bolted joints because the clamped plate thickness was 2 mm. The washer's thickness was set thicker than normal because we increased the grip length of the bolted joint to accurately measure the clamp force F and also to make clear the difference of contact area A_w for each bolted joint.

3.2 Shear tensile test

Figure 3 shows a tensile test situation for the bolted joint. Figure 3a depicts a front view of the clamped plates, while Fig. 3b shows the tensile test situation, which includes an extensometer. The clamp plates were 100 mm long, 25 mm wide, and 2 mm thick. They were made of cold-rolled steel plate. The two clamped plates were tightened with the test bolt and nut, and the clamp force F was controlled using the strain gage after setting the washers. We did not lubricate the mating surfaces between the clamped plates, the thread surfaces, or the bearing surface of the bolted joint at all. The extensometer was positioned 25 mm from the bolt axis, and three strain gages were attached to the clamped plates as shown in Fig. 3b.

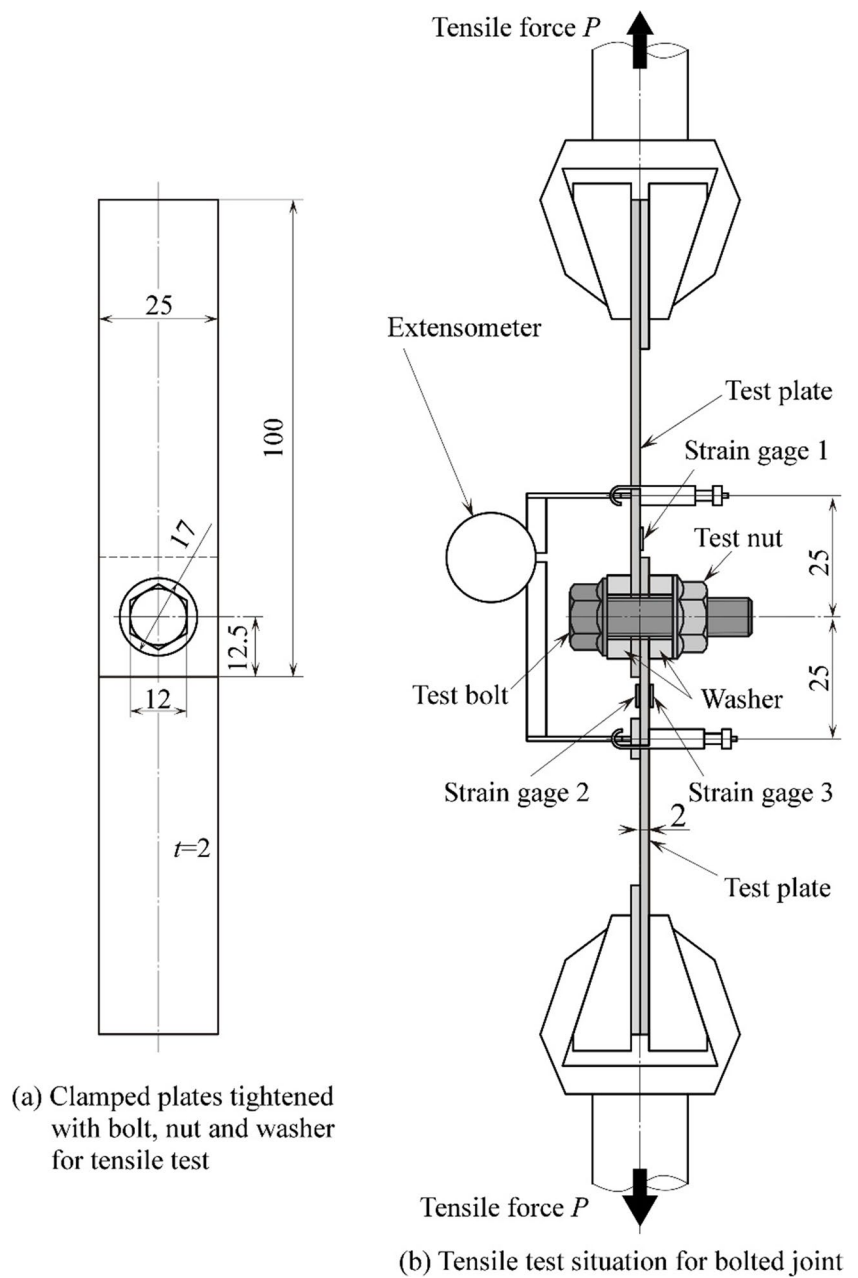
The tensile tests were conducted using the following procedure. After the two clamped plates were initially pulled until the maximum tensile force $P_{\max} = 2.2$ kN, the tensile force was reversed to zero. This cycle was repeated four times. The maximum tensile force $P_{\max} = 2.2$ kN was determined via preliminary experiments not to exceed point B in Fig. 1b. The reason why we repeated it was to confirm behaviors of the shear stiffness and slippage between the clamped plates under cyclic load.

At first, we investigated the effects of clamp force on the shear stiffness of bolted joint I in this study. The clamp forces F_i , measured in kilonewtons, were set to the four cases, $F_i = 3$ kN, 4 kN, 5 kN, and 6 kN as shown in Table 1. Next, we investigated the effects of contact area between washers and clamped plates on their shear stiffness using all types of bolted joint. The contact area A for each joint is listed in Table 2. Finally, we investigated the effects of the roughness of the washer surface contacting the clamped plates on their shear stiffness, as shown in Table 3. Each surface roughness was prepared by polishing the surface with sandpaper #120, #600, and #2000 and measured using a surface roughness tester. The actual surface roughness R_a varied slightly between each bolted joint.

3.3 Finite element model

Figure 4 shows four finite element analysis (FE analysis) models that are the same shapes as the four types of bolted joints shown in Fig. 2. The bolt models and the nut models have spiral screw threads. The thread shape, bolt, and the nut were made based on ISO 68-1 [31]. The shapes of the clamped plates and washers were the same as in Fig. 2 and Fig. 3. The FE analyses were conducted with completely elastically models. Young's modulus E and Poisson's ratio ν of the bolt, nut, clamped parts, and washers were set to E

Fig. 3 Schematic illustration of shear tensile test for bolted joints



= 206 GPa and $\nu = 0.3$ respectively. The thermal expansion coefficient of the washers was defined as $\alpha = 1.17 \times 10^{-5}$ 1/K to generate the clamp force F . The clamp force was

set as shown in Table 1. The friction coefficient between contact surfaces was $\mu = 0.25$. The left clamped plate was constrained as shown in Fig. 4, and the right side of the

Table 1 Experimental condition to investigate an effect of clamp force

Bolted joint type	Clamp force F (kN)
Bolted joint I	3
Bolted joint I	4
Bolted joint I	5
Bolted joint I	6

Table 2 Contact area between clamed plates and washers

Clamp force F (kN)	Bolted joint type	Contact area A (mm ²)
6	Bolted joint I	170
6	Bolted joint II	351
6	Bolted joint III	42.2
6	Bolted joint IV	478

Table 3 Surface roughness of washer after polished

Bolted joint type	Polish	Average roughness R_a (μm)
Bolted joint I	Polished by #120	0.74
	Polished by #600	0.22
	Polished by #2000	0.08
Bolted joint III	Polished by #120	0.34
	Polished by #600	0.16
	Polished by #2000	0.10
Bolted joint IV	Polished by #120	0.59
	Polished by #600	0.14
	Polished by #2000	0.08

clamped plate was pulled at tensile force P . The elastic finite element analyses were conducted using Marc Mentat 2021.1.

We conducted FE analysis to investigate the effects of clamp force on their shear stiffness as in the original experiments shown in Table 1. We then investigated the effects of contact area between washers and clamped plates on their shear stiffness using all types of bolted joint through FE analysis, as seen in Table 2. Although we wanted to investigate the effects of surface roughness between the washer surface and the clamped plate surfaces, as demonstrated in Table 3, it was difficult to simulate the differences in surface roughness. Consequently, we conducted FE analysis varying the friction coefficients, as shown in Table 4 to simulate the difference in surface roughness.

4 Results and discussions

4.1 Behaviors of bolted joint receiving shear force

Figure 5 shows behaviors of the tensile force P versus the strain ε_2 and ε_3 at each position of strain gage 2 and 3 for bolted joint I in the experiment and FE analysis. The clamp force F_i was 6 kN. It also shows the behavior of tensile force P versus tensile strain ε_t measured by the strain gage and calculated by FE analysis. In Fig. 5, the ordinate shows the tensile force P , and the abscissa shows each strain. The gray curves show the relationships in two cycles as measured in the experiments, and the dotted curves show the relationships calculated by FE analysis. The tensile force P versus the strain ε_m between the measurement length measured by the extensometer and calculated by FE analysis is also shown by the gray curve and the dotted curve in Fig. 5. The tensile strain ε_t was calculated using the following equation as an average of ε_2 and ε_3 .

$$\varepsilon_t = \frac{\varepsilon_3 + \varepsilon_2}{2} \quad (4)$$

The strains ε_m between the measurement length l_m (=50 mm) measured by the extensometer and calculated by FE analysis was calculated using the following equation.

$$\varepsilon_m = \frac{x_m}{l_m} \quad (5)$$

where x_m is the elongation between the measurement length.

It can be seen in Fig. 5 that the tensile force P behavior versus strain ε_2 and ε_3 in the FE analysis almost accurately expresses that of the experiments. The tensile force P behavior versus the tensile strain ε_t in the FE analysis could also capture the tensile force P behavior in the experiments. However, the tensile force P behavior versus the strain ε_m between the measurement length l_m was slightly different in the experiment and the FE analysis. This may be due to slight differences in the deformations of the clamped plates (including bolt and nut) in the experiment and the FE analysis, as the bolted joint includes several contact points. The inclination of P versus ε_m in the initial region of the experiment was almost the same as the inclination of P versus ε_t , which may be that attitude indicates that it is contributed to thermal expansion coefficients, the set value of frictional coefficient μ in the FE analysis, or other boundary conditions. Nevertheless, it can be concluded that the FE analysis could reasonably capture the real phenomenon of the bolted joint.

In Fig. 5, the inclination of P versus ε_m in the initial region of the experiment corresponds to 0-A in Fig. 1. It can be seen that slippage hardly ever occurred between the clamped plates at that time because the relationship between P and ε_m is linear. Hence, we defined the inclination of the tensile force P versus the elongation x_m between the measurement length l_m in this region as the shear stiffness k_i of the bolted joint. The shear stiffness of the bolted joint k_i is expressed using the following equation.

$$k_i = \frac{P}{x_m} \quad (6)$$

where i in the shear stiffness k_i indicates a loading cycle turn because we conducted four cycles in the experiment. Namely, k_1 indicates the shear stiffness in the first cycle. Since the inclination of P versus x_m at the starting point of the experiments was a little unstable, we derived the shear stiffness k using the range from $P = 0.5$ to 1.0 kN.

Following this, the slippage occurred between the clamped plate, and the bolt deformed into an S shape in area A-B of Fig. 1. Furthermore, section B-C shows a region where the bearing surface under the bolt head and nut as

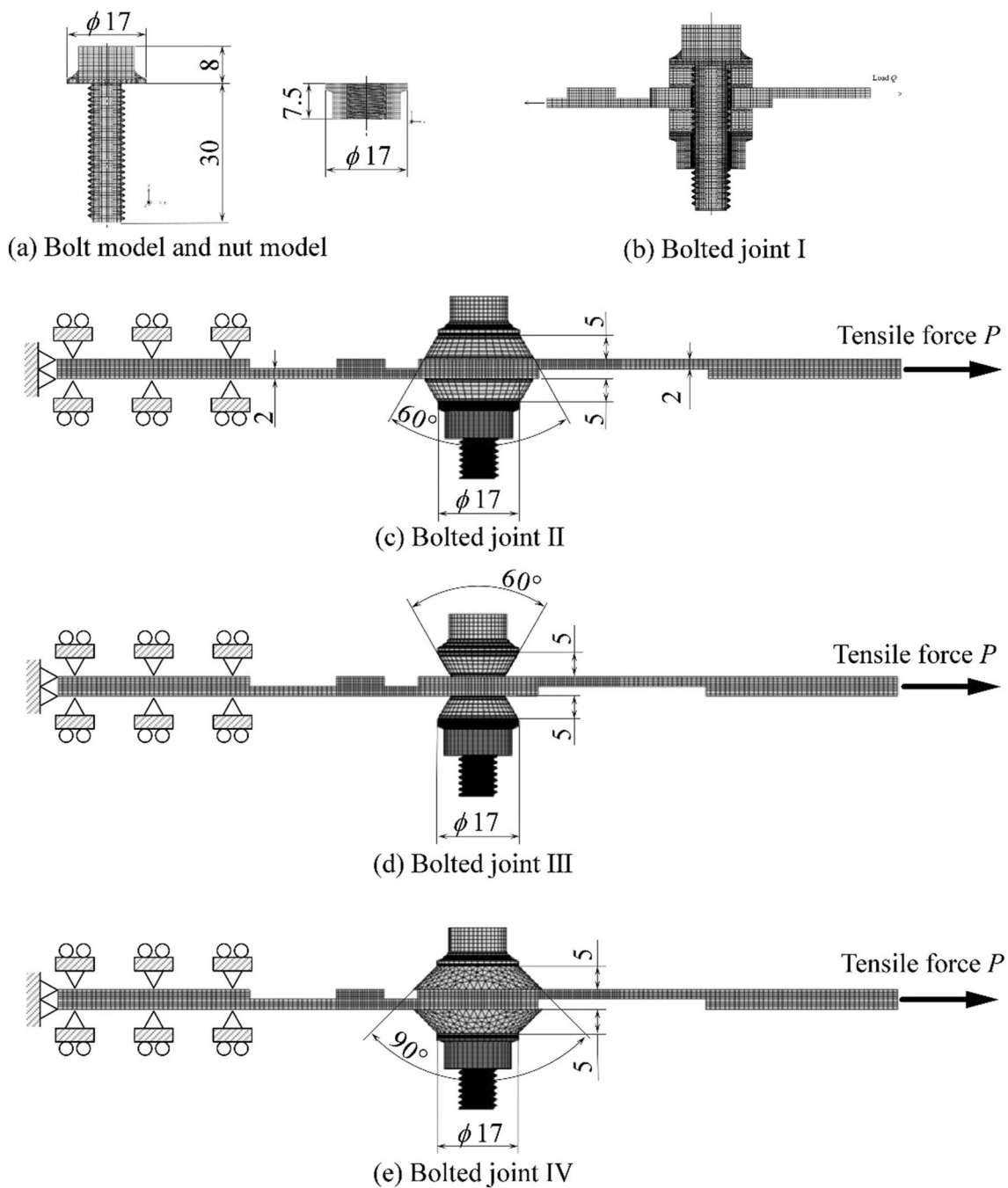


Fig. 4 FE models of bolted joints with different washer types

Table 4 Friction coefficients in FE analysis

Bolted joint type	Clamping force F (kN)	Friction coefficient μ
Bolted joint I	6	0.10
Bolted joint I	6	0.25
Bolted joint I	6	0.40

well as the engaging thread surfaces started to slip. In Fig. 5, the tensile force P in the unloading process decreased linearly, and the behavior of P in the second cycle showed a linear relation not only during the loading process but also during the unloading process. This result indicates that after the slippage between the clamped parts occurred in the first loading process, the displacement due to the slippage between the clamped plates would never return to the original even when P was unloaded.

Fig. 5 Examples of shear tensile test result and FE analysis results of bolted joint I

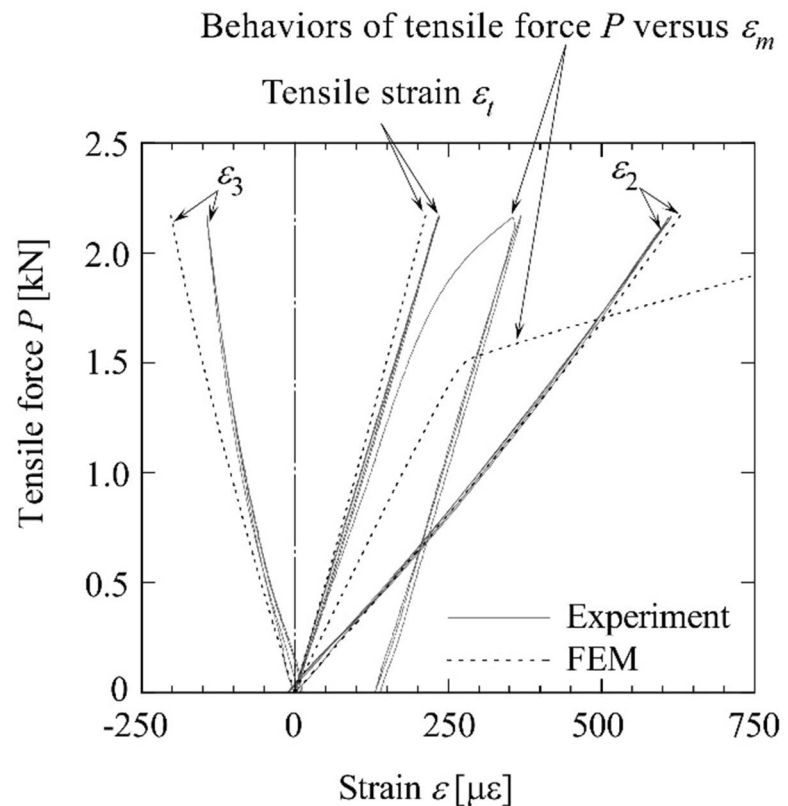
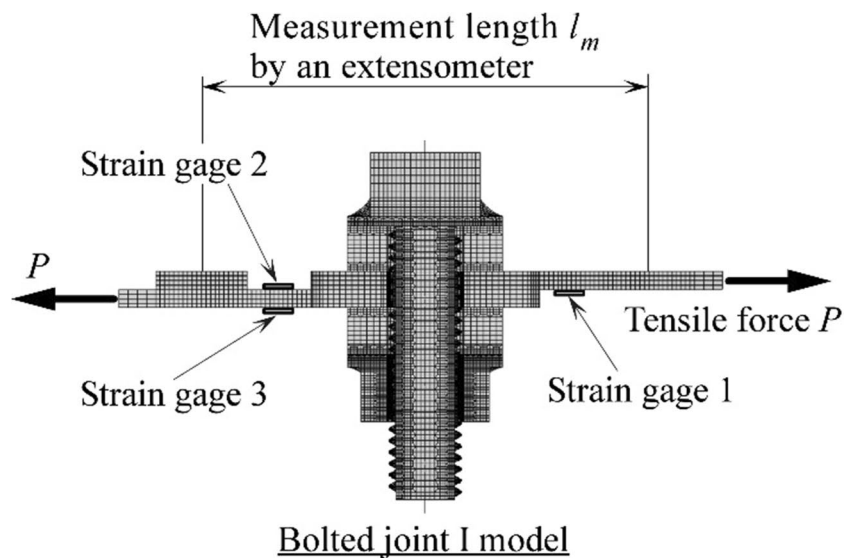
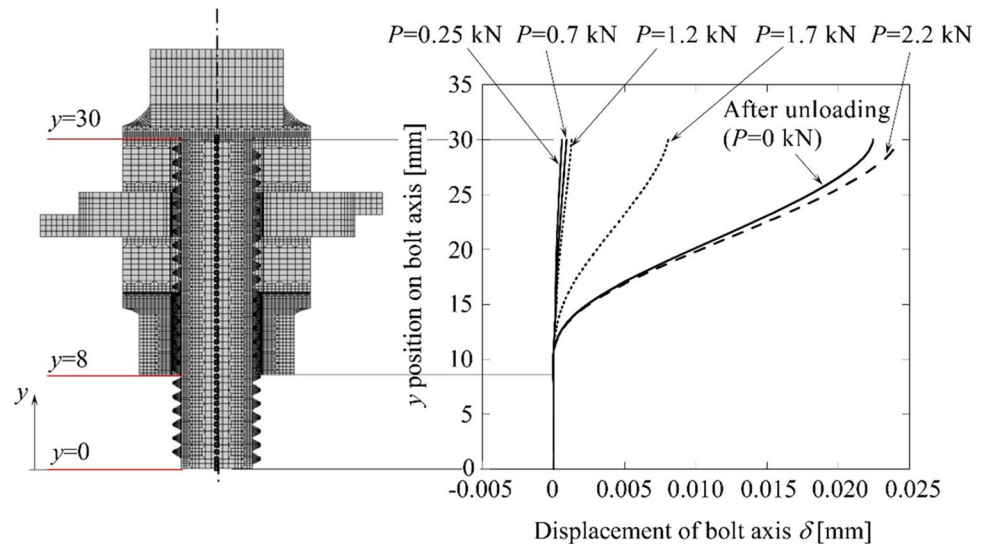


Figure 6 shows deformation shapes at bolt axis of bolted joint I when the bolted joint received each tensile force P in FE analysis. In Fig. 6, the ordinate shows y position in the bolt axis, and the abscissa shows the deformation δ of the bolt axis in the shear direction. The deformations δ of the bolt axis were calculated as the difference between the displacement of bolt axis in shear direction at each y position and the inclined line based on a line connected from $y = 0$ to $y = 8$ on bolt tip.

Figure 6 shows that all deformation shapes at each tensile force P were S-shaped, and the deformations δ increased with an increase in the tensile force. Although the deformations δ slightly increased, they rapidly increased after P exceeded 1.2 kN. After the tensile force P was released to 0 kN, the deformation did not return to its original position. These results indicate that the bolted joint deformation up until $P = 1.2$ kN was due to elastic deformation of the bolted joint, including elongation of the clamped plates. The reason that

Fig. 6 Bolt axis deformation δ when bolted joint pulled by several shear forces P simulated by FE analysis



the displacement δ greatly increased at the bolt neck portion after the tensile force P exceeded 1.2 kN is that slippage significantly occurred between the clamped parts. And the reason that the displacement δ at bolt neck portion did not return to the original position even after releasing the tensile force P is considered to be that the friction force between the clamped plates was larger than the recovery force due to the elastic deformation of the bolt. This phenomenon was confirmed in Fig. 5. Therefore, it can be concluded that even when the bolted joint receives cyclic shear tensile force P only in the tensile direction, slippage will occur between the clamped parts at the first cycle, and they will never return to their original positions.

Figure 7 shows the distributions of contact stress p calculated by FE analysis between the clamped parts on both sides of the bolt. The contact stress p is the value at the centerline of the wide direction. The left diagram shows the contact stress p between the clamped parts on the left side of the bolt, and the right diagram shows the same thing on the right side. In the diagrams, the ordinate is the contact stress p , and the abscissa is position x from the bolt axis. It can be seen in Fig. 7 that the contact area decreases with an increase in the tensile force P . This is due to the separation at the edges between the clamped plates. Therefore, this result indicates that the bolted joint has rotated to the clockwise direction due to the tensile force P .

4.2 Effect of number of loading cycles on shear stiffness

Figure 8 illustrates the shear stiffness of bolted joint I in the experiment and FE analysis, with a clamp force F_i of 6 kN. Figure 8a displays the relationship between the tensile force P and displacement δ at the measurement length l_m in the experiment and FE analysis. Figure 8b shows the shear stiffness k during loading process and unloading process at each

cycle in the experiments. In Fig. 8a, the black line shows the experimental result, and the dotted line shows the FE analysis result. It can be seen in Fig. 8a that there is a difference between the inclinations of the experiment and FE analysis. This difference is also shown in Fig. 5 and is attributed to FE analysis not being able to perfectly simulate the deformations of the bolted joint due to its multiple contact portions. As mentioned above, the shear stiffness k was measured in the range between $P = 0.5$ and 1.0 kN as the behavior of tensile force P less than 0.5 kN was unstable in several experiments. In Fig. 8a, the proportional limit of the tensile force P in the first cycle was defined as P_1 , determined as the tensile force P at the plastic strain was generated 0.0005%. In this study, we have also estimated the linear limit P_1 in addition to the shear stiffness k in each condition. Incidentally, as it can be seen in the relationship between the tensile force P and the displacement δ in Fig. 8a, the macroscopic slippage did not occur between the clamped plates in and after the second cycle. As the cause, it is difficult to consider that the bolt shank touched the bolt hole because the displacement δ of the clamped plates was less than 0.02 mm. Hence, it is considered as the result that the contacting surfaces of the clamped plates were running in due to the first slippage. The result indicates that we can increase the proportional limit P_1 at which the clamped plates start to slip by means of letting the contacting surfaces of the clamped plates run in before use.

The shear stiffness k_i in the three experiments is shown in Fig. 8b. The abscissa shows the number of loading cycles, and the ordinate shows the shear stiffness k_i . The error bars drawn with solid lines show the scatter bands during the loading process in the three experiments, and the dotted error bars show the scatter bands during the unloading process. The white circular symbols and the black circular symbols show those averages respectively. In addition, the

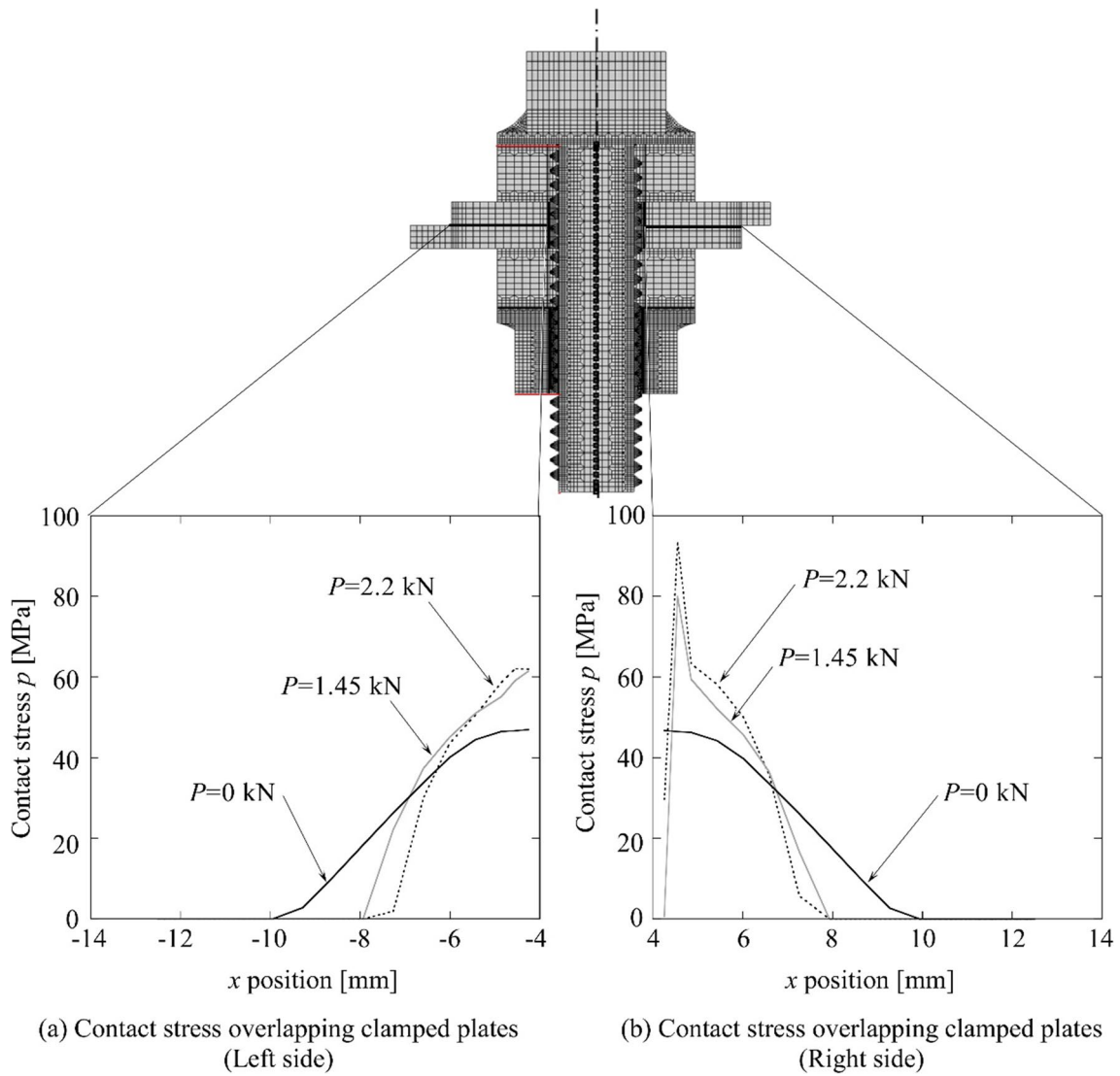
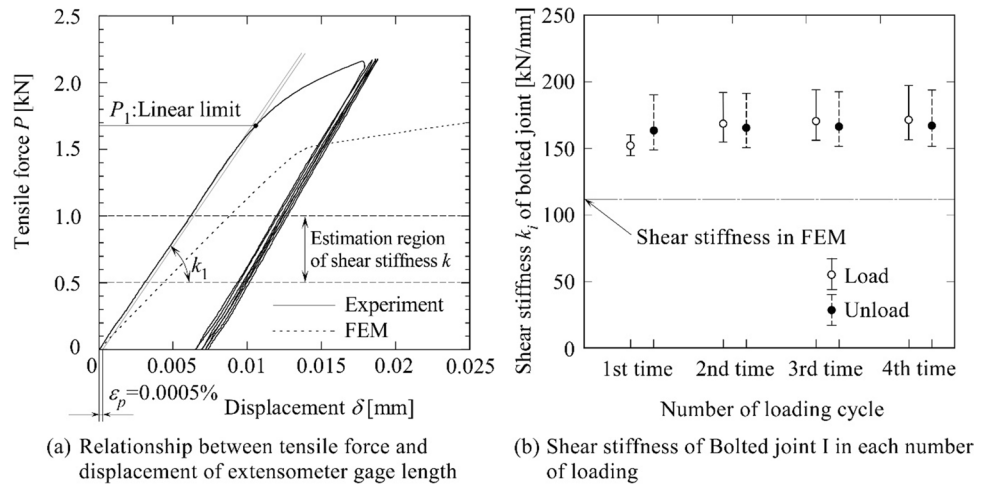


Fig. 7 Contact stress p between overlapped clamped plates when bolted joints subjected to shear forces P simulated by FE analysis

Fig. 8 Examples of relationship between tensile force P and displacement δ and shear stiffness in case for bolted joint I



shear stiffness k_1 calculated by FE analysis was shown by the dotted line.

It can be seen in Fig. 8b that the shear stiffness k_i apart from that of the first loading cycle was almost constant in spite of the loading and unloading. As can be seen in Fig. 8a, since significant slippage occurred between the clamped parts only during first loading cycle, it is believed that the shear stiffness k_1 in the first cycle was slight lower than that in other cycles. From these results, it can be concluded that the shear stiffness k_i for the entire loading and unloading cycle was approximately 150 kN/mm, and there was no significant change for each loading and unloading cycle. However, the shear stiffness k_1 calculated by FE analysis was approximately 110 kN/mm. As mentioned above, the discrepancy between the experimental shear stiffness and the analytical shear stiffness is likely due to the slight difference in the deformation and slippage of the clamped plates, including the bolt and nut between the experiment and the FE analysis since the bolted joint incorporates multiple contact points.

Incidentally, the tensile stiffness of only the clamped plate can be calculated as follows.

$$k_{\text{plate}} = \frac{E \cdot A}{l_m} = \frac{206 \times 10^9 \cdot 0.025 \times 0.002}{0.05} = 206 \times 10^6 \text{ N/m} = 206 \text{ kN/mm} \tag{7}$$

where E is Young’s modulus and A is a cross sectional area of the clamped plate.

It is observed that the tensile stiffness of the clamped plate alone was approximately 15% higher than the experimental shear stiffness k of bolted joint I. The lower shear stiffness of the bolted joint can be attributed the increase in localized strain caused by stress concentration at the edges of the bolt head and nut, as well as the rotation of the joint as previously discussed.

4.3 Effect of clamp force on shear stiffness

Figure 9 shows the effect of clamp force F_i on the shear stiffness k_1 and the proportional limit P_1 of the tensile force in the first loading cycle in the experiments and FE analysis. Figure 9a shows the relationship between F_i and k_1 , and Fig. 9b shows the relationship between F_i and P_1 . In Fig. 9a, b, the black circular symbols and the error bars show the experimental results, and the gray circular symbols show k_1 calculated by FE analysis. As can be seen in Fig. 9a, the shear stiffness k_1 in the first loading cycle gradually increased with an increase in the clamp force F_i , and the increasing trend agrees with FE analysis although the absolute values of k_1 differ at each clamp force. However, the proportional limit P_1 was widely scattered when the clamp force F_i was low. P_1 in the FE analysis increased with an increase in the clamp force. Just focusing on the average value of P_1 in the experimental results, P_1 from $F_i = 3$ to 5 kN in the experiments also increased with an increase in the clamp force, similar to the FE analysis although the average value of P_1 when $F_i = 6$ kN in the experimental results slightly decreased. Therefore, although there are some differences between the experimental results and the FE analysis results, both phenomena concur. The reason that P_1 scattered widely when F_i was low may be due to the instability and influence of slight waviness errors between the mating surface of clamped parts, as the friction force between the clamped plates when F_i was low was small.

4.4 Effect of contact area on shear stiffness

Figure 10 shows the effect of contact area A on the shear stiffness k_1 and the proportional limit P_1 of the tensile force in the first loading cycle in the experiments and FE analysis. Figure 10a illustrates the relationship between F_i and k_1 , and Fig. 10b shows the relationship between F_i and P_1 . The

Fig. 9 Influences of clamp force on shear stiffness of bolted joint (bolted joint I)

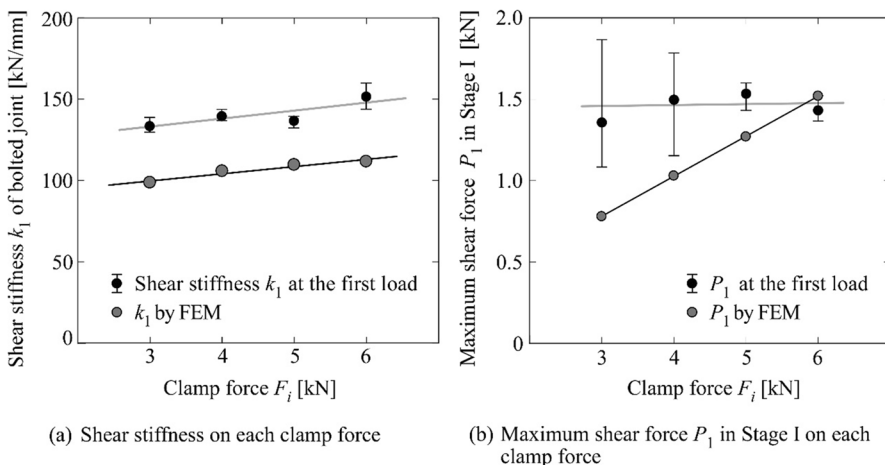
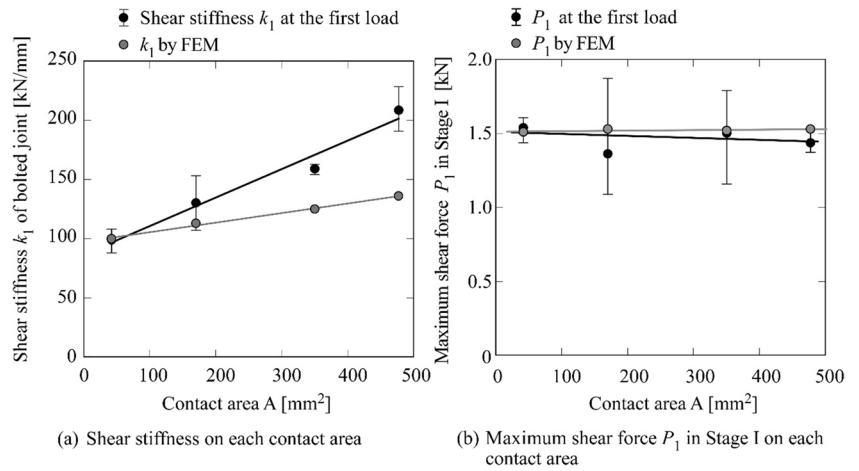


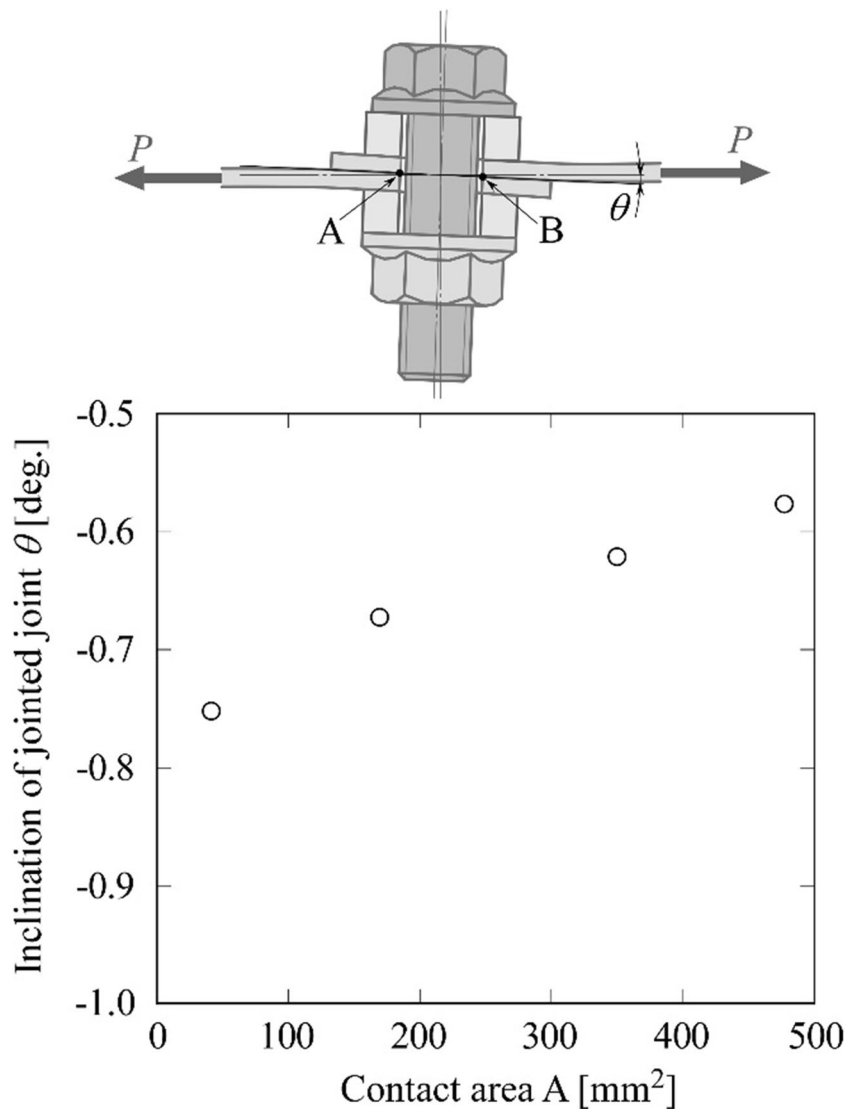
Fig. 10 Influences of contact area between clamped plate and washer on shear stiffness of bolted joint



black circular symbols and the error bars in Fig. 10 show the same as in Fig. 9. It is seen in Fig. 10a that the shear stiffness k_1 gradually increased with an increase in the contact

area A , and the increasing trend agreed with FE analysis. However, the increasing ratios of the experiments and FE analysis were slightly different for each contact area A . The

Fig. 11 FEM relationship between contact area and inclination of plate



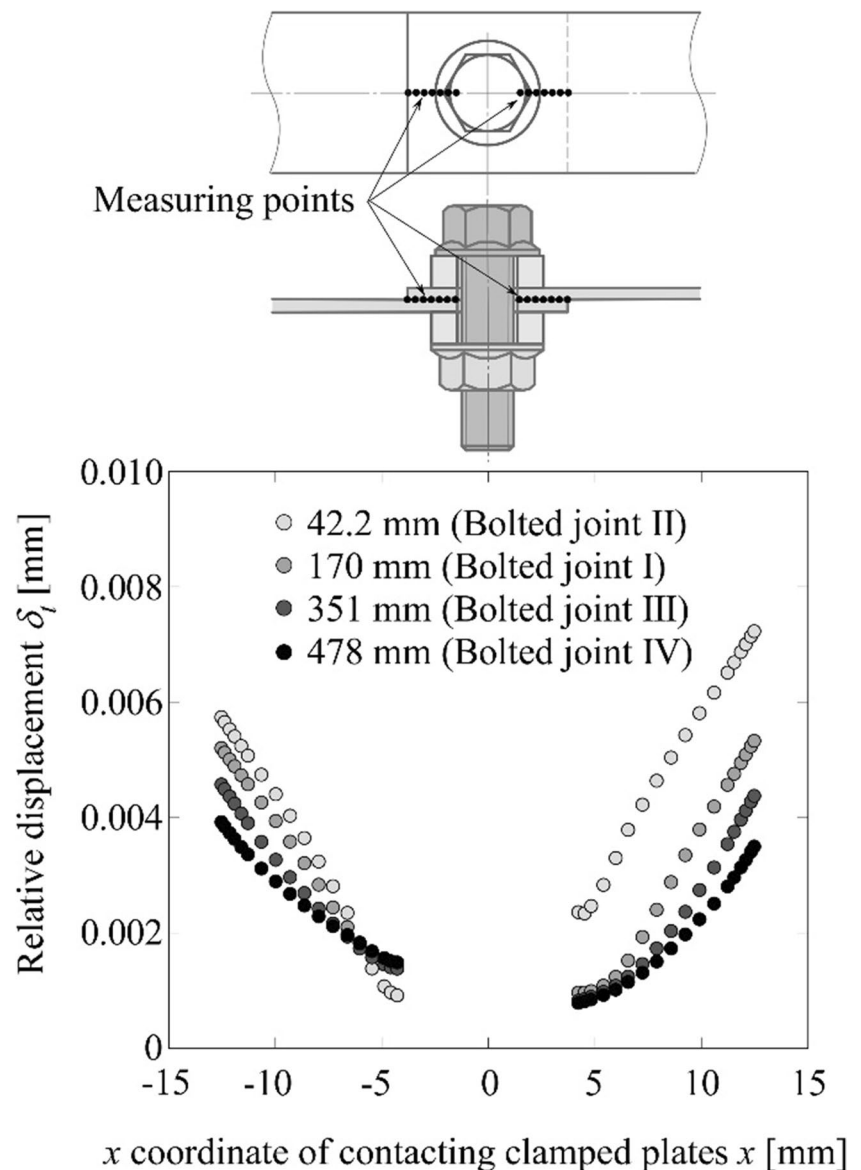
behaviors of the proportional limit P_1 were almost the same in the experiments and FE analysis although the experimental values scattered widely for bolted joints I and II.

Figure 11 shows the relationship between the size of the contact area A and the inclination θ due to rotational deformation of the bolted joints in FE analysis. In Fig. 11, the ordinate shows the inclination θ , and the abscissa shows the size of the contact area A . The inclination θ was defined as the inclination between points A and B. Figure 11 illustrates that the inclination θ due to rotational deformation of the bolted joints increases with a decrease in the size of the contact area A . The results indicate that the contact area A increases the bending stiffness of the bolted joints, and the increase of the bending stiffness induced the shear stiffness k_1 of bolted joints.

Figure 12 shows the relative displacement δ_i on position x of the overlapped clamped plates shown in the upper figure. The ordinate is relative displacement δ_i corresponding to the slippage between the clamped plates, and the abscissa is the position x of the overlapped clamped plates. The relative displacements δ_i in the same tensile force P correspond to the shear stiffness k_1 of bolted joints. It was observed that the relative displacements δ_i decreased with an increase in the size of the contact area A , and the relative displacements δ_i significantly depended on the size of the contact area A . Thus, it can be seen that the contact area A is a key factor for increasing the shear stiffness of the bolted joints under the same tensile force P .

From these results, it was seen that an increase of the size of the contact area between the clamped plates reduced the

Fig. 12 Relative displacement corresponding to slippage between clamped plates



deformation rotation of the bolted joints due to shear load. It was also seen that the reduction of the deformation rotation of the bolted joints made the shear stiffness k_1 increase. Therefore, it is considered that bolted joint IV of which the size of the contact area A was the largest was the optimum washer in order to increase the shear stiffness. The result shows that the shear stiffness depends not only on the slip resistance between the clamped plates but also on the size of the contact surface between the washers and clamped plates and the inclination due to rotational deformation of the bolted joint. The results indicate that we can increase the shear stiffness of lap-jointed plates in the spot welding and other joining techniques by considering spot positions to avoid the deformation rotation of the joint portion.

4.5 Effect of surface roughness on shear stiffness

Figure 13 shows the effect of surface roughness R_a of contacting surfaces of clamped plates on the shear stiffness k_1 in the first loading cycle on the experiments shown in Table 3. The ordinate shows the shear stiffness k_1 , and the abscissa shows the surface roughness R_a of the contacting surfaces of clamped plates. It can be observed that the shear stiffness k_1 decreased with an increase in the surface roughness R_a for bolted joints III and IV. But the shear stiffness k_1 for bolted joint I remained nearly constant despite changes in the surface roughness R_a . If it is assumed that the friction coefficient increases with an increase in the surface roughness, an increase of the friction coefficient might have reduced the shear stiffness k_1 .

It is not easy to simulate the surface roughness. However, if the differences in surface roughness can be assumed to be the differences in the friction coefficient, we can comparatively easily conduct FE analysis by changing the friction coefficient between the clamped plates. Thus, an FE analysis which varied the friction coefficient between the clamped plates was conducted for bolted joint I in Table 4. Figure 14a shows the effect of friction coefficient μ between clamped plates on the shear stiffness k_1 in the FE analysis. Additionally, Fig. 14b illustrates the behaviors of the proportional limit P_1 of the tensile force versus the friction coefficient μ . In the simulations, since P_1 for $\mu = 0.1$ was less than 1.0 kN as shown in Fig. 14b, the shear stiffness k_1 for just $\mu = 0.1$ was estimated to be between $P = 0.1$ and 0.6 kN.

Figure 14a shows that, while the effect of the friction coefficient μ on the shear stiffness k_1 was not very remarkable, the shear stiffness k_1 increased slightly depending on the friction coefficient μ . The result of the FE model—bolted joint I—agreed with the experimental results. The results indicate that although an increase in the friction coefficient μ could be expected to lead to an increase in k_1 , this was not the case. In Fig. 13, the shear stiffness

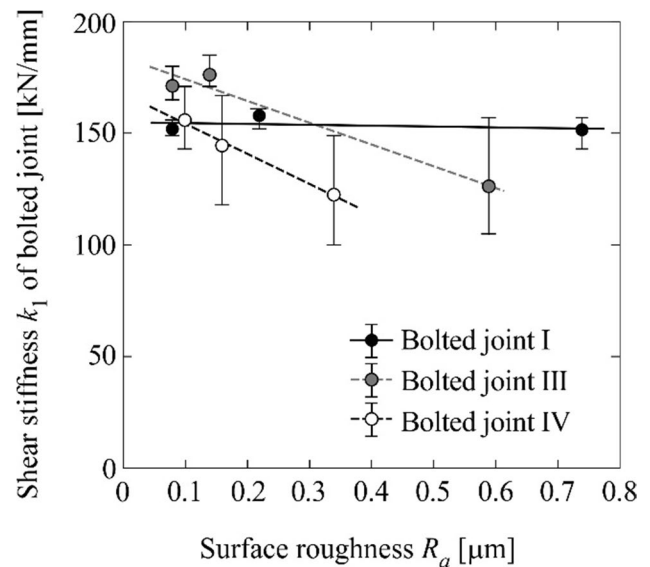


Fig. 13 Influence of surface roughness between contacting surfaces of clamped plate on shear stiffness of bolted joint

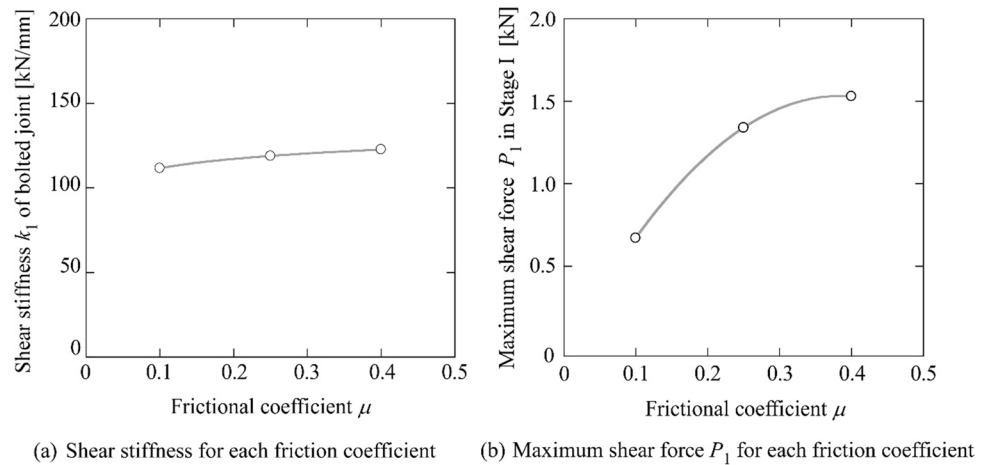
k_1 for bolted joint I did not change with an increase in surface roughness R_a , but k_1 decreased with an increase in R_a for bolted joints III and IV. If it had been assumed that the friction coefficient μ increases with an increase in the surface roughness R_a , even for bolted joint I, the FE analysis would have predicted an increase in k_1 . However, the results of FE analysis were counter to the assumption. Therefore, the results show that we cannot apply the assumption that the friction coefficient μ should increase with an increase in surface roughness R_a in this case. For bolted joints III and IV, it is difficult to understand why the shear stiffness k_1 decreased. Further research is therefore necessary to determine what caused the surface roughness to reduce the shear stiffness k_1 .

5 Conclusions

We investigated the deformation mechanism of bolted joint subjected to shear load and the effects of washer shape and several parameters on the shear stiffness of bolted joints in experiments and FE analysis. Our conclusions are as follows.

1. When shear force was repeatedly loaded and unloaded on the bolted joints, the shear stiffness in the first cycle was slight lower than that in other cycles, but the shear stiffness after the second cycle almost did not change. The proportional limits of shear force after the second cycle were higher than that in the first cycle. Consequently, it is considered that we can increase the pro-

Fig. 14 Influence of friction coefficient between clamped plate on shear stiffness of bolted joint (FEM)



proportional limit at which the clamped plates start to slip by means of letting the mating surfaces of the clamped plates be running in before use.

- It was seen that the shear stiffness depended on the clamp force experimentally and analytically. It was also seen that the proportional limits of shear force in the first cycle tended to depend on clamp force although the proportional limits in the experiments scattered widely.
- The shear stiffness gradually increased with an increase in the size of the contact area between the clamped plates. But the increasing ratios of the shear stiffness in the experiments and FE analysis were slightly different in each contact area. The proportional limits were almost the same independent of the contact area.
- The effect of the surface roughness between the clamped plates on the shear stiffness was not clear in the experiments, but the shear stiffness slightly increased depending on the friction coefficient between the clamped plates in FE analysis. If it was assumed that the friction coefficient increased with an increase in the surface roughness, the results did not agree. Therefore, we have to continue the investigation with regard to the effect of the surface roughness.
- The increase of contact area lets the inclination due to rotational deformation of the bolted joint decrease, and the decrease of the inclination lets the shear stiffness increase. Therefore, if we can decrease the inclination by considering joint positions, we can increase the shear stiffness except for increasing the contact surface. Since this can apply on the spot welding and so on, we are going to discuss joint positions and let the inclination decrease in the future step.

Author contributions All authors contributed to the study conception, design, material preparation, data collection, and analysis. The

first draft of the manuscript was written by Shinji Hashimura, and all authors commented on previous versions of the manuscript. All authors read and approved the final manuscript.

Declarations

As the corresponding author, I, Shinji Hashimura, hereby confirm on behalf of all authors that:

Competing interests The authors declare no competing interests.

Open Access This article is licensed under a Creative Commons Attribution 4.0 International License, which permits use, sharing, adaptation, distribution and reproduction in any medium or format, as long as you give appropriate credit to the original author(s) and the source, provide a link to the Creative Commons licence, and indicate if changes were made. The images or other third party material in this article are included in the article's Creative Commons licence, unless indicated otherwise in a credit line to the material. If material is not included in the article's Creative Commons licence and your intended use is not permitted by statutory regulation or exceeds the permitted use, you will need to obtain permission directly from the copyright holder. To view a copy of this licence, visit <http://creativecommons.org/licenses/by/4.0/>.

References

- Anami T (2016) Aluminum Applications for automotive body and next generation automobiles. *J Surf Finish Soc Japan* 67(12):639–643
- Meschut G, Janzen V, Olfermann T (2014) Innovative and highly productive joining technologies for multi-material lightweight car body structures. *J Mater Eng Perform* 23(5):1515
- Morodomi H, Nishihara Y, Matsubara S, Hashimura S, Hori H (2020) A study of high-speed joining method using spiral nails. *J Manuf Proc* 59:500
- Shah U, Liu X (2019) Effects of ultrasonic vibration on resistance spot welding of transformation induced plasticity steel 780 to aluminum alloy AA6061. *Mater Des* 182(108053):1–11. <https://doi.org/10.1016/j.matdes.2019.108053>
- Wang Y, Tao W, Yang S (2019) A method for improving joint strength of resistance spot welds of AA 5182-O aluminum alloy. *J Manuf Proc* 45:661–669. <https://doi.org/10.1016/j.jmapro.2019.07.024>

6. Abe Y, Ishihata S, Maeda T, Mori K (2018) Mechanical clinching process using preforming of lower sheet for improvement of joinability. *Proc Manuf* 15:1360–1367. <https://doi.org/10.1016/j.promfg.2018.07.347>
7. Hashimura S, Miki T, Otsu T, Komatsu K, Inoue S, Yamashita S, Omiya Y (2020) Robustness of polyisobutylene for friction coefficients between bearing surfaces of bolted joints. *Proc IMechE Part J: J Eng Tribol* 234(1):50
8. Hashimura S, Kamibeppu K, Nutahara T, Fukuda K, Miyashita Y (2019) Effects of clamp force on fatigue strength of aluminum alloy bolts. *Proc Struct Integr* 19:204–213
9. Yoshimoto, I., (1983) A Hypothesis concerning fatigue strength of a bolt-nut joints, *J Japan Soc Precis Eng* 49-6, 801-803.
10. Schwerdt D, Pyttel B, Berger C (2011) Fatigue strength and mechanisms of wrought aluminium alloy in the VHCF-region considering material and component relevant influencing factors. *Int J Fatigue* 33:31
11. Yamamoto A (1978) On the self-loosening mechanism of threaded fasteners. *J Soc Mech Eng* 81(716):617–622
12. Kasei S, Ishimura M, Ohashi N (1988) On self-loosening of threaded joints in the case of absence of macroscopic bearing-surface sliding - loosening mechanism under transversely repeated force. *J Japan Soc Precis Eng* 54(7):1381–1386
13. Izumi S, Yokoyama T, Iwasaki A, Sakai S (2005) Three-dimensional finite element analysis of tightening and loosening mechanism of threaded fastener. *Eng Failure Anal* 12(4):604–615
14. Pai NG, Hess DP (2002) Experimental study of loosening of threaded fasteners due to dynamic shear load. *J Sound Vibr* 253(3):585–602
15. Pai NG, Hess DP (2002) Three-dimensional finite element analysis of threaded fastener loosening due to dynamic shear load. *Eng Failure Anal* 9(4):383–402
16. Zhang M, Lu L, Wang W, Zeng D (2018) The roles of thread wear on self-loosening behavior of bolted joints under transverse cyclic loading. *Wear* 394-395:30–39
17. Hashimura S, Komatsu K, Otsu T, Sekido Y (2017) Influences of lubricants and bearing surface configuration under bolt head on self-loosening of bolted joints. *Tribol* 62(3):205–216
18. Dravid S, Tripathi K, Chouksey M (2014) Role of washers in controlling loosening of full threaded bolted joints. *Proc Technol* 14:543
19. Pirdayr A, Mohammadi M, Kazemzadeh-Parsi MJ, Rajabi M (2021) Self-loosening effects on vibration characteristics of plates with bolted joints: an experimental and finite element analysis. *Measurement* 185(109922). <https://doi.org/10.1016/j.measurement.2021.109922>
20. Zhao B, Wu F, Sun K, Mu X, Zhang Y, Sun Q (2021) Study on tangential stiffness nonlinear softening of bolted joint in friction-sliding process. *Tribol Int* 156:106856
21. Fukuoka T, Nomura M, Morimoto, (2006) Proposition of Helical Thread Modeling with Accurate Geometry and Finite Element Analysis. *Trans. of Japanese Society of Mechanical Engineers, Series A* 72(723):1639–45
22. Fukuoka T, Nomura M, Yasui D (2020) Numerical analysis of loosening phenomena of bolted joints under shear loads using helical thread models. *J Japan Inst Mar Eng* 55(4):522–528
23. Fukuoka T, Nomura M, Fuchigami T (2009) Finite element analysis of the fatigue strength of threaded fasteners using helical thread models. *Trans. Japanese Soc Mech Eng Series A* 75(759):1570–1576
24. Hashimura S, Socie D (2005) A study of loosening and fatigue of bolted joints under transverse vibration. *SAE Tech Paper*. <https://doi.org/10.4271/2005-01-1320>
25. Hashimura, S. and Kurakake, Y., A study to predict fatigue limits of bolted joints under transverse vibration, *SAE Technical Paper* 2010-01-0964, 2010, <https://doi.org/10.4271/2010-01-0964>
26. Soomro IA, Pedapati SR, Awang M (2022) A review of advances in resistance spot welding of automotive sheet steels: emerging methods to improve joint mechanical performance. *Int J Adv Manuf Technol* 118:1335–1366
27. Song H, Yang C, Yang N, Li K, Chen Z (2021) Research on a multidimensional strain energy estimation method for welding spots based on performance optimization. *Int J Adv Manuf Technol* 117:1263–1273
28. Abdollahzadeh A, Bagheri B Advances in simulation and experimental study on intermetallic formation and thermomechanical evolution of Al–Cu composite with Zn interlayer: effect of spot pass and shoulder diameter during the pinless friction stir spot welding process. *Proc Inst Mech Eng Part L: J Mater Des Appl*. <https://doi.org/10.1177/14644207221146981>
29. Bagheri B, Abbasi M, Givi M (2019) Effects of vibration on microstructure and thermal properties of friction stir spot welded (FSSW) aluminum alloy (Al5083). *Int J Precis Eng Manuf* 20:1219
30. Asati B, Shajan N, Kishore AVT, Arora KS, Narayanan RG (2022) A comparative investigation on self-piercing riveting and resistance spot welding of automotive grade dissimilar galvanized steel sheets. *Int J Adv Manuf Technol* 123:1079–1097. <https://doi.org/10.1007/s00170-022-10226-y>
31. ISO 68-1 (1998) ISO general purpose screw threads - Basic profile - Part 1: Metric screw threads. International Organization of Standardization

Publisher's note Springer Nature remains neutral with regard to jurisdictional claims in published maps and institutional affiliations.